In silico structure-function analysis of pathological variation in the HSD11B2 gene sequence

American Physiological Society | Physiological Genomics

PUBLISHED ARTICLE
ARCHIVES
SUBSCRIPTIONS
SUBMISSIONS
CONTACT US

Physiol Genomics. 2010 August; 42(3): 319–330. PMCID: PMC2929884
Published online 2010 June 22. doi: 10.1152/physiolgenomics.00053.2010

In silico structure-function analysis of pathological variation in the *HSD11B2* gene sequence

Jonathan R. Manning,[1] Matthew A. Bailey,[1] Dinesh C. Soares,[2] Donald R. Dunbar,[1] and John J. Mullins[1]

[1]Centre for Cardiovascular Science, Queen's Medical Research Institute and
[2]Medical Genetics Section, Molecular Medicine Centre, Institute of Genetics and Molecular Medicine, Western General Hospital, University of Edinburgh, Edinburgh, United Kingdom

Corresponding author.

Address for reprint requests and other correspondence: J. R. Manning, Centre for Cardiovascular Science, Queen's Medical Research Inst., Univ. of Edinburgh, Edinburgh EH14 4TJ, UK (e-mail: jmanning@staffmail.ed.ac.uk).

Received March 18, 2010; Accepted June 15, 2010.

Abstract

11β-Hydroxysteroid dehydrogenase type 2 (11βHSD2) is a short-chain dehydrogenase/reductase (SDR) responsible for inactivating cortisol and preventing its binding to the mineralocorticoid receptor (MR). Nonfunctional mutations in *HSD11B2*, the gene encoding 11βHSD2, cause the hypertensive syndrome of apparent mineralocorticoid excess (AME). Like other such Mendelian disorders, AME is rare but has nevertheless helped to illuminate principles fundamental to the regulation of blood pressure. Furthermore, polymorphisms in *HSD11B2* have been associated with salt sensitivity, a major risk factor for cardiovascular mortality. It is therefore highly likely that sequence variation in *HSD11B2*, having subtle functional ramifications, will affect blood pressure in the wider population. In this study, a three-dimensional homology model of 11βHSD2 was created and used to hypothesize the functional consequences in terms of protein structure of published mutations in *HSD11B2*. This approach underscored the strong genotype-phenotype correlation of AME: severe forms of the disease, associated with little in vivo enzyme activity, arise from mutations occurring in invariant alignment positions. These were predicted to exert gross structural changes in the protein. In contrast, those mutations causing a mild clinical phenotype were in less conserved regions of the protein that were predicted to be relatively more tolerant to substitution. Finally, a number of pathogenic mutations are shown to be associated with regions predicted to participate in dimer formation, and in protein stabilization, which may therefore suggest molecular mechanisms of disease.

Keywords: apparent mineralocorticoid excess, homology modeling

THE MINERALOCORTICOID RECEPTOR (MR) has equal affinity for aldosterone and the main glucocorticoid, cortisol (5). Cortisol circulates at 100–1,000 times higher concentration than aldosterone, and specificity of MR in mineralocorticoid target tissues is due to colocalization of the receptor with the

enzyme 11β-hydroxysteroid dehydrogenase type 2 (11βHSD2) (24). 11βHSD2 catalyzes the conversion of the MR ligand cortisol to cortisone, which does not activate the receptor (see Fig. 1).

11βHSD2 has an important role in the physiological regulation of blood pressure, and loss-of-function mutations in the encoding gene, *HSD11B2*, cause the syndrome of apparent mineralocorticoid excess (AME; OMIM +218030), characterized by hypokalemia and low-renin hypertension (14, 21, 45, 49). Fewer than 100 cases of AME, mostly children, have been reported worldwide. However, it is highly likely that the severity of AME precludes an accurate estimation of prevalence. AME causes a failure to thrive, and in a mouse model of the disease 50% of individuals die within 48 h of birth because of complications associated with severe potassium wasting (34). A mild form of AME (OMIM 207765) has been described in which enzyme activity is reduced, rather than ablated (38, 61, 66). However, the strong correlation between disease phenotype and underlying enzyme activity militates against subclassification into distinct variants and indicates that AME is a continuum disorder. Indeed, polymorphisms in *HSD11B2* have positive associations with either blood pressure per se or salt sensitivity of blood pressure (1, 2, 13, 40, 43, 54, 65), and as such it is an attractive candidate gene for hypertension in the general population. Given that subtle changes in coding and noncoding regions may well contribute to an elevation of blood pressure, predicting the functional ramifications of sequence variation is of considerable interest.

11βHSD2 is a 405-amino acid, 42-kDa (11, 12) member of the “short-chain dehydrogenase/reductase” (SDR) family of NAD- or NADP-dependent oxidoreductases, a large protein family with 73 documented members in the human genome (see Ref. 10 for review). SDRs are diverse, including epimerases and dehydratases (53), and pairwise identities between family members are low. Since there are no high-resolution experimentally determined three-dimensional structures for 11βHSD2, a structure-based analysis necessitates generation of a homology model. The closest relative to 11βHSD2 is 17βHSD2 (38% identity over 387 alignable residues, E value = 2e-63), which also lacks a solved structure. A model previously generated for 17βHSD2 was used as the basis for a model employed to investigate cofactor binding in 11βHSD2 (4). Cofactor preference of 11βHSD2 was thereby shown to be due primarily to Glu115, which provided steric and coulombic repulsion with the adenosine ribose phosphate group. Asp91 was also implicated and shown to provide important stabilizing interactions with other residues.

17βHSD1, a more distant relative of 11βHSD2 than 17βHSD2 (26% identity over 346 alignable residues, E value of 9e-16), which does have a resolved structure, was used in conjunction with a model of glucose dehydrogenase to hypothesize a structure for 11βHSD2 (12). This model was used to examine the functional impact of an Asp to Asn mutation in 11βHSD2 at residue 223. These models were either unavailable or unsuitable for the present study because of low definition outside the authors' region of interest. We have generated a new predicted structure of 11βHSD2 based on 17βHSD1 in order to interpret the functional consequences of AME-associated mutations in *HSD11B2*.

MATERIALS AND METHODS

Extraction of Known 11βHSD2 Mutations

A manual search of the literature identified all currently known natural and engineered mutations in 11βHSD2 and correlated them, where possible, with enzyme activity.

Interpretation of a Multiple Sequence Alignment

The multiple sequence alignment for Ensembl (30) protein family ENSFM00500000270244,

containing 11βHSD2s and the paralogous 17βHSD2s, was downloaded and filtered down to nine species: human, chimpanzee, mouse, rat, zebra fish, frog, cow, pig, and chicken. This alignment provides a resource of information on the structural and functional constraints experienced by equivalent positions between protein structures. Gene duplication events produce paralogous groups of genes with related but distinct functions—caused by different selection pressures on function—but with similar structural constraints. Assuming sufficient substitution has occurred since the common ancestor of a pair of sequences, positions significant for protein structure or function are expected to exhibit global or clade-specific conservation. Patterns of substitution between the orthologs of human 11βHSD2 were examined and compared with those of the 17βHSD2s.

Fold Recognition, Template Selection, and Target-Template Alignment

A fold recognition search of the human 11βHSD2 sequence by PHYRE (32) expectedly revealed that the sequence was compatible with an oxidoreductase/NAD(P)-binding/Rossmann-fold domain; all of the top 10 “hits” had very high confidence scores (E value < 10^{-40}; estimated precision = 100%). The sequence of human 11βHSD2 was input to BLASTP (3), applied against the Protein Data Bank (PDB) (8), identifying a 17βHSD1 structure [PDB ID: 1JTV; 1.54 (25)] as the best template, with an E value of 9e-16. The PROMALS3D server (39) was employed to produce an alignment of 11βHSD2 against the template structure and other related sequences. From this, manual refinements were made to the target-template alignment to avoid placement of gaps in locations that would disrupt large secondary structure elements predicted from sequence or template homology (in many cases equivalent; see Fig. 3).

Incorporation of Ligands

Ligands were incorporated into the template structure with PyMol (18). The SDR structure is well conserved in the cofactor-binding domain, although there are cofactor-dependent variations. NAD was added via superposition of xylitol dehydrogenase [PDB ID: 1ZEM (19)], which was crystallized with NAD. Models were created incorporating the entire xylitol dehydrogenase cofactor-binding domain as an additional template for modeling, but this produced inferior models. In addition, the testosterone ligand in 1JTV was replaced with cortisol, obtained from the PDB and structurally overlaid with testosterone. It was observed (25) that androgens such as testosterone (C19 steroids) bound to 17βHSD1 in the opposite orientation when compared with estrogens (C18). Rotating cortisol into an estrogen-like orientation produced a clash with the predicted cofactor position, so an androgen orientation was assumed. Given the substantial differences between 11βHSD2 and 17βHSD1 in this region, a different placement is possible.

Modeling

Modeling was performed using Modeller 9v6 (55). The dimer interface was inherited from the modified template structure. NAD was modeled explicitly by Modeller, while cortisol was considered as a rigid body with minimal participation in the modeling process. Fifty models were generated, from which the best was selected on the basis of packing and stereochemical assessments. Modeller's internal “DOPE” score (56) was employed to rank models, and from among the top-scoring 50% models assessments were made for stereochemistry (dihedral statistics) in the form of Ramachandran plots (41), model validity assessed with ProQ (63) and Verify3D (42), and coarse packing quality evaluated with WHAT IF (62). Additional analysis of packing and stereochemistry was carried out by use of RAMPAGE (41).

Refinement

Where the model did not fit with known important regions in the loops that bind NAD, refinements were made to the starting alignment and the model was recalculated.

Analysis

Known pathogenic mutations of 11βHSD2 were mapped onto the model structure and interpreted in the context of existing structure-function data. Secondary structures for template and model were defined by use of Stride (23). Atoms were defined as "in contact" if their predicted separation was <0.5 plus their respective van der Waals radii. Polar contacts were identified by use of routines from PyMol. (*Caveat lector*: Inaccuracies are likely, particularly at the COOH-terminal end of the molecule where similarity with the template is low.)

RESULTS AND DISCUSSION

Comparison with Related Sequences

NADP-dependent 11βHSD1, despite substrate similarity, shares only 23% identity with NAD-dependent 11βHSD2 over 302 alignable residues and has a predicted single membrane helix (compared to 3 in 11βHSD2), producing an endoplasmic reticulum-luminal localization of the catalytic domains, opposite to 11βHSD2's cytoplasmic orientation (51).

A multiple sequence alignment was constructed in order to examine positional constraints on substitution in 11βHSD2. Because of the inherent diversity of the SDR family, producing a reliable alignment can be difficult. To ensure as accurate an alignment as possible a group of 11βHSD2 orthologs was compared with a closely related paralogous group of orthologs, the 17βHSD2s. While 17βHSD2s also lack a solved crystal structure, the high sequence similarity to 11βHSD2s (and resultant high-reliability alignment) ensures that conservation-based inferences in the following discussion are reliable. The alignment, shown in Fig. 2, forms the basis of subsequent discussion.

Prediction of 11βHSD2 Protein Structure

The closest homologue in the PDB to 11βHSD2 was human 17βHSD1, available under PDB identifiers 1IOL (7) and 1JTV (25) and a close match with an E value of 9e-16. Although a previous model based on this template (12) was kindly made available to us, the substrate binding residues were outside the original region of interest and were therefore not well defined, so we have generated a new model.

The resolution of 1JTV (1.54) was higher than that of 1IOL (2.30), and hence it was employed as the primary template. However, this structure was incomplete, lacking solved residues after Thr190 (1JTV numbering) that is present in the 1IOL structure. This fragment from 1IOL was therefore included when modeling this region.

11βHSD2 is believed to form dimers (28), so the existing dimeric quaternary structure of the template's biological assembly was deemed suitable for modeling. Functionally, dimer formation in 11βHSD2 may be necessary for enzyme activity, and its disruption may be responsible for a lack of activity in homogenates (50). This fits well with observations in 17βHSD1 (employed here as template), in which the active unit is a dimer (35), but seems to be in contradiction to other experiments that suggested an inhibitory role for dimer formation in 11βHSD2 (28). Whatever the mechanisms involved, dimerization seems to be important for function, and its disruption may therefore lead to pathological consequences.

Figure 3 shows the sequence alignment of 11βHSD2 with those residues of the template sequence present in the solved structure (residues 81–368), a JPred (15)-predicted secondary structure for 11βHSD2, and the Stride-derived (23) secondary structures of 17βHSD1. The probable NH -terminal

helices are evident in an unaligned region. The high content of conformationally important proline and glycine residues in the COOH-terminal unaligned region of 11βHSD2 is indicative of disorder, which may explain the absence of solved amino acid residues in this region for homologous structures.

Quality assessment of model structure. Examination of the model by use of a Ramachandran plot in RAMPAGE (41) showed that 93% of modeled main chain positions have "favored" conformations, with only 2% retaining incorrect geometry. This is acceptable and indicates that the model stereochemistry is of good quality. Similarly, the LGscore (16) and MaxSub scores for the model, obtained from the ProQ server (63), indicated a very (3.810) or fairly good (0.393) model, respectively. The mean three-dimensional profile score for the model derived from Verify3D (42), which measures the compatibility of a sequence with a proposed structure, was 0.33, comparing favorably with the template's score of 0.51. Below-zero smoothed scores, indicating problematic modeling, occurred only at, or adjacent to, regions lacking template-derived constraints (residues 274–290 and 106–107).

Poor packing of amino acids is often an indication of poor prediction of amino acid side chain orientation, and this was assessed with the coarse packing quality metric available in WHAT IF (62). This produced an average overall quality control score of −1.067. To place this in context, incorrect models give scores of less than −3.0, lower-quality models less than −2.0; and the average quality of 235 highly refined X-ray structures was −0.59 (±0.4) (62). Only 10 or 9 residues of 288 modeled residues, in chains A and B, respectively, fall below the −5.00 threshold that would indicate significant problems in packing. These occur almost exclusively in loop regions of the model where homology between query and template is especially low.

Figure 4 shows the proposed placement of NAD and cortisol ligands within the model, with two chains arranged in a dimeric fashion with reference to the PQS-derived (29) dimer structure of 17βHSD1, and highlights regions of low confidence in the model. L114 of chain A exhibits poor packing, but being located in the ligand or cofactor binding sites this may relate to the structural constraints specific to ligand binding and hence may not necessarily indicate poor modeling. Of the remaining problematic regions, many occur in loops between secondary structure elements, which are poorly modeled because of low identity with the template. In particular, the 274–290 loop region highlighted as problematic by Verify3D contains a large insertion relative to the template.

Documented AME-Associated 11βHSD2 Mutations

Table 1 presents all known nonsynonymous mutations in 11βHSD2, which result in AME or hypertension. R337C was the first such discovery (68), found in three homozygous siblings with AME, and was followed quickly by several more homozygous mutations from multiple families (67). Compound heterozygotes (R208H,R337H+ΔY338) with AME were later identified (33, 46), and reduced 11βHSD2 activity in patients was demonstrated for both homozygotes and compound heterozygotes (R213C, Y232S, truncation) (46). In addition to point changes in protein sequence, mutations leading to truncated proteins were also found in two siblings with AME and a stillbirth (59).

Variable phenotypic impact of mutation. Not all mutations in the *HSD11B2* gene lead to full-blown AME pathology and/or inactive enzyme. A patient homozygous for P227L showed only modestly (42%) reduced cortisol to cortisone conversion (66). The R279C mutation (38) also had mild biochemical phenotype—albeit with typical AME presentation. Mutations S180F, A237V, and A328V were all shown to have significant levels of partial activity when expressed in whole cells, while L179R and R208H were inactive (47). Defects in the enzyme activity of 11βHSD2 or perturbed cortisol metabolism has been demonstrated in the heterozygous parents of AME patients with homozygous 11βHSD2 mutations (44,

58), which sometimes lead to mild, late-onset hypertension. In particular, this has been demonstrated for A328V (37) and ΔL114+E115 (52).

Impact of mutation on stability. Reduced protein stability rather than reduced catalysis was shown to be the cause of reduced 11βHSD2 activity for positions 335–339 (6) (associated with rapid protein degradation at the proteasome) and for COOH-terminal truncated forms (50).

Noncoding mutations. A number of other genetic determinants of often milder disease symptoms have been found associated with *HSD11B2*, including untranslated region (UTR) elements (36) and polymorphisms (1, 9, 13, 57, 65), but are not pertinent to the present structural discussion.

Structural and Functional Implications of 11βHSD2 Mutations

Known pathogenic mutations of 11βHSD2 were interpreted on the basis of their structural context in the 11βHSD2 model, conservation with related sequences, and existing functional knowledge from the available literature. Figure 5 shows placement of these mutations in the model structure and highlights Arg279 (in white). Arg279 was indicated as problematic for sequence-structure compatibility by Verify3D (42) and for packing by WHAT IF (62), probably because of location in a region of low template homology close to an insertion in 11βHSD2 relative to 17βHSD1.

Mutated positions proximal to ligand or cofactor binding regions. Figure 6 shows those pathogenic mutations occurring close to the ligand or cofactor binding regions, and whose mutation is likely to impact directly on enzyme activity. Of the residues shown, Tyr232, Lys236, Leu114, Glu115, and Asp91 have well-documented impacts on enzyme function and/or cofactor binding (4, 48, 52). Leu114 makes hydrophobic contacts with the NAD cofactor, a role fulfilled by an arginine residue in the template structure, which also provides a positive charge to facilitate binding of the phosphate in NADP. Glu115 has a key role in defining substrate specificity for NAD over NADP (4), most probably via coulombic repulsion. Asp91 may be critical for stabilizing the conformations of a number of residues important for cofactor binding (4). The side chain of Tyr226 (36) lies within 3 of the predicted position of the substrate, so mutation is likely to disrupt ligand binding. Pro227 mutations (P227L, P227N) probably have related effects, since P227 creates a “kink” important to maintain the structural positioning of Tyr226.

Mutated positions with possible implications for protein stability. Mutations that do not directly affect substrate or cofactor binding can disrupt protein function. For example, the R337C mutation reduces stability of 11βHSD2 (20), and variants lacking a nonconserved COOH-terminal peptide have increased protein turnover (50). Similarly, experiments in heterologous expression systems have suggested that the S180F, A237V, and A328V mutants have reduced stability (47). Protein destabilization has been shown to be the root cause of reduced enzyme activity for a number of pathogenic and artificial mutations in the residue 335–339 range (6). R337C and Y338H were completely inactive, as were all mutants of Tyr338. Subcellular location suggestive of misfolding was shown for Y338H, as well as recovery of activity in conditions favoring increased stability.

Figure 7 shows the predicted positions in structure of the known stability-associated residues of 11βHSD2. The 335–339 cluster occurs in proximity to a COOH-terminal region (347–368) of the second chain of the model, assigned a helix-loop-helix arrangement by reference to the 17βHSD1 template as part of the dimer interface (Fig. 7, *bottom left*). The spatial arrangement of interactions between numerous disease-associated positions is reproduced from those of the 17βHSD1 template, and is likely a core structural feature of this protein family. The hydroxyl group of Y338 makes a hydrogen bond with the main chain of R335, and its bulky ring system lies in close proximity to A328, supporting

a hydrophobic interaction. In the process, a kink is introduced (also present in the template structure) that causes arginines 335–337 to project outward from the loop, toward one of the long supporting helices of the structure, and the other dimer. Tyrosine is the only amino acid that has the hydrophobic bulk to generate this kink together with a hydrogen bonding potential, which may explain the total inactivation observed when this position is mutated. The pathogenic and functional impact of the relatively conservative A328V mutation (37) is consistent with a core structural context and associated tight packing for Ala328. Arg213 (46), located in a β-strand of the central β-sheet of the structure, seems to anchor this loop via a number of hydrogen bonds that would be disrupted in R213C.

Differences with the template make inferences more tentative for other positions in this region. The equivalent residue to Arg337 in the template, Arg252 (see Fig. 3), is involved in intrachain polar interactions with the side chains of Glu163 and Glu167 and main chain atoms of the other subunit at Pro270. In the model there is a predicted deletion relative to the template where a Pro270-equivalent residue would otherwise be. This shortens the interhelix loop, and Glu163 and Glu167 are substituted with Ala240 and Asp244, respectively, seemingly precluding interaction with Arg337, which may instead form interchain contacts (see below). Asp244 (mutated in D244N) is predicted to participate in an ionic interaction with residue Arg336 (template L251) that lies within the aforementioned positively charged cluster (residues 335–339), while the main chain of Ala240 makes an H-bond with the side chain of Asp244.

D223Q causes impaired cofactor and ligand binding (12), and D223 is suggested to hydrogen bond to Gln261 in the β-strand adjacent to that containing Arg337. R359W lies in the speculative helix-loop-helix region of the structure COOH terminus close to the 335–339 cluster and may participate in interchain interactions. A requirement for such interactions may be the cause of a preponderance of polar residues among 11βHSD2 sequences at this position (Fig. 2, column 378), in contrast to 17βHSD2s. Mutations L376P and R374Term occur close to the COOH terminus, with potential impact on stability as with COOH-terminal truncated forms (50), similarly for a frameshift mutation from position 356 (67).

A final mutation with probable structural significance, but distant from the above-discussed region, is Leu250 [associated with the L250R (17) and L250P (67) mutations], absolutely conserved between all the 11βHSD2s and 17βHSD2s in Fig. 2 (column 263). Leu250 projects away from the dimer interface into a highly hydrophobic environment, suggesting a position of core structural significance and therefore likely to produce disrupted structures in mutant forms.

Other mutated positions occurring at predicted dimer interface. Potential interchain contacts form another set of known pathogenic mutations in 11βHSD2 (Fig. 8), some of which overlap with the stability-associated set. S180F (template Leu102), R186C (template Ala108), R208H (template Ly130), and R337C (template Arg252) all occur at positions associated with predicted hydrogen bonds that may be disrupted in mutant proteins. Ser180 is predicted to participate in an interchain hydrogen bond involving its main chain with Lys201, analogous to a Leu102-Gln123 bond in the template. The side chain of Ser180 projects intrachain, and the increase in bulk of S180F is likely to displace this region and disrupt interaction—in addition to other structural ramifications. A237V (template Val332) and L251S (template Leu174) are predicted to occur close to hydrophobic positions of the other chain, which might disrupt the dimer interface by increasing side chain bulk (A237V) or polarity (L251S). The side chain of Tyr299 [deleted in 1 case of AME (39)] occurs close to the interchain interface. The model suggests an interchain hydrogen bond for Arg337 with Tyr353 in the less well-modeled COOH-terminal helix-loop-helix.

The dimer interface is composed in part of a helix that supports the critically important positions Lys236 and Tyr232, as well as Ala237, Asp244, and Leu251. Without further experiment it is impossible to determine whether potential impact on dimerization competence or active site disruption is responsible for the observed phenotypic effects. However, the position of many of these residues in orientations facing the other subunit is suggestive of the former possibility.

It has been suggested (50) that the reduced activity of mutant enzymes in cell homogenates (e.g., Ref. 47; see Table 1) reflects reduced competence for oligomerization. This is in line with the majority of research on mammalian SDRs, which suggests that interfacial structural assemblies are essential for active site integrity and activity (26, 27), and fits with observations of pathogenic mutations close to the dimer interface. One study (28) produced the surprising conclusion that physiologically 11βHSD2 was inactivated on dimer formation, a result that, given the bulk of SDR research, is in need of confirmation. If proved correct, an “active monomer” scenario would need to be reconciled with the pathogenic nature of interfacial mutations. A possibility would be that the dimeric form acts as a degradation-resistant reservoir of latent enzyme that on dissociation produces a transient burst of activity before proteasomal degradation. A structural disruption impairing dimerization would then cause constitutive rapid degradation and low-level activity. This admittedly speculative theory could be supported by our *in silico* observation that AME mutations having a demonstrable effect on protein stability lie close to the dimer interface.

Other mutated positions in structure. Two remaining positions in the model, Arg279 [associated with R279C (38)] and Leu179 (L179R mutation) (Fig. 9) are associated with pathogenic mutations. Arg279 lies surface-exposed in a short helix after the sixth β-strand, and was noted by WHAT IF (62) to have problematic packing in the model, making inferences based on likely interactions difficult. However, the pathology of Arg279 is relatively mild [mild AME/late-onset hypertension (38)], and the mutant protein retains high partial activity in vitro, which is consistent with relatively minor structural/functional disruptions. Leu179 is more buried and lies in a loop after short fourth helix, exhibiting likely hydrophobic contacts with a number of positions including Leu291 and Lys280. Given this positioning, we anticipate that L179R would disrupt packing and greatly reduce protein function, leading to a more severe disease phenotype than R279C.

Nonpathogenic mutations. Five missense mutations in 11βHSD2, L14F, R74H, R147H, T156I, and R335H, were initially identified in hypertensive members of the Japanese population (31). All these mutations were found in the heterozygous state in both the hypertensive and wider normotensive population, and are therefore likely to have more subtle effects on protein function. Leu14 and Arg74 occur in the membrane-anchor region of the sequence and therefore are not represented in the model structure. Arg335 is part of the 335–339 stability-associated cluster and has been previously shown to be tolerant to conservative mutation (6). The T156I mutation is placed in a loop after the third helix, while the relatively conservative R147H occurs in a helix. Both of these positions are distant from important regions described so far, such as the ligand-binding and interchain regions. Heterozygosity for relatively conservative mutations may explain their lack of severe pathogenic phenotype.

Limitations. Inferences based on homology models are by their nature tentative. Disease-assignment mutation predictions based on homology models reduce in accuracy where query-template identity is <30% (68). This is a result of less reliable side chain interactions arising from higher main chain position errors, an increased frequency of sequence alignment errors, and a higher number of insertions and deletions. In addition, modeling of the “loops” without homologous template-guided restraints becomes less accurate as loop length increases (22).

In the present study the manually curated query-template alignment shows few “long” gaps, none of which correspond to the mutated positions of interest, that occur predominantly in regions with clear template homology. The conservation of secondary structure elements and demonstrated favorable scores for geometry and packing further mitigate any potential issues. The consequences of mutation described in the present study, therefore, while still putative, are likely to be reliable.

Summary and Concluding Remarks

We have examined the available literature on known mutations in the *HSD11B2* gene and assessed them in the context of existing data and their position on a constructed three-dimensional homology model for its encoded protein.

Mutations, phenotypic severity, and conservation. Mutations that cause a reduction in protein function or expression are likely to have minor consequences relative to those that abolish enzyme activity altogether. In general terms, nonsynonymous mutations associated with severe phenotypes are expected to impact strongly on protein structure and/or function and be selected against. As a result, the associated positions exhibit nonpermissive patterns of substitution when compared between orthologous sequences.

In patients with homozygous mutations, and where the resultant mutant proteins have been consistently shown to be inactive (R208H and L179R), the associated positions of the alignment in Fig. 2 (221 and 192, respectively) are invariant across the alignment. The mutations at these positions might be expected to introduce gross structural rearrangements that abolish function. For three nonconservative mutations for which clinical phenotype was reported as being particularly mild even in a homozygote/compound heterozygote state, P227L (Fig. 2, pos 240), R279C (Fig. 2, pos 298), and R359W (Fig. 2, pos 378), significantly less global conservation was present—although P227, for example, is strongly conserved in 11βHSD2s. The positions are evidently more tolerant to substitution, and accordingly mutations introduce more subtle changes to structure and function—which is in agreement with their relatively peripheral posited location in structure as discussed in RESULTS.

A recurring theme in the literature of 11βHSD2 mutations is the role of protein degradation. We have suggested that mutations previously shown to lead to more rapid turnover can be used to implicate proximal positions in our model in a “guilt by association” approach. This degradation-associated region is also close to the predicted dimer interface, where further AME-associated mutations are located. Combined with observations of the impact of dimer formation on 11βHSD2 activity, this may provide circumstantial evidence pointing to a role for dimer formation in maintaining 11βHSD2 stability.

Many recent studies have implicated reduced 11βHSD2 function in syndromes related to AME, but of much milder phenotype, including late-onset hypertension and salt sensitivity. The recent discovery of subtle effects on transcription via promoter polymorphism (2), and its impact on salt sensitivity, are of particular interest. The association of mild-phenotype with heterozygous nonsynonymous, as well as noncoding mutations and polymorphisms with disease, may have implications for a much wider section of the population than those affected by the rare syndrome of AME. It is likely that further research will yield a larger set of subclinical 11βHSD2 mutations that, when characterized, will yield further information on this protein's structure and function.

GRANTS

J. R. Manning and D. R. Dunbar were funded by a British Heart Foundation Centre of Research

Excellence Award. J. J. Mullins is a recipient of a Wellcome Trust Principal Research Fellowship. M. A. Bailey was a Wellcome Trust Intermediate Fellow. D. C. Soares was funded by the Wellcome Trust.

DISCLOSURES

No conflicts of interest, financial or otherwise, are declared by the author(s).

ACKNOWLEDGMENTS

We are grateful to Christopher Kenyon for helpful advice and to Louise Evans for her contribution of Fig. 1.

REFERENCES

1. Agarwal AK, Giacchetti G, Lavery G, Nikkila H, Palermo M, Ricketts M, McTernan C, Bianchi G, Manunta P, Strazzullo P, Mantero F, White PC, Stewart PM. CA-repeat polymorphism in intron 1 of HSD11B2: effects on gene expression and salt sensitivity. Hypertension 36: 187–194, 2000. [PubMed: 10948076]

2. Alikhani-Koupaei R, Fouladkou F, Fustier P, Cenni B, Sharma AM, Deter H, Frey BM, Frey FJ. Identification of polymorphisms in the human 11beta-hydroxysteroid dehydrogenase type 2 gene promoter: functional characterization and relevance for salt sensitivity. FASEB J 21: 3618–3628, 2007. [PubMed: 17551100]

3. Altschul SF, Gish W, Miller W, Myers EW, Lipman DJ. Basic local alignment search tool. J Mol Biol 215: 403–410, 1990. [PubMed: 2231712]

4. Arnold P, Tam S, Yan L, Baker ME, Frey FJ, Odermatt A. Glutamate-115 renders specificity of human 11beta-hydroxysteroid dehydrogenase type 2 for the cofactor NAD^+. Mol Cell Endocrinol 201: 177–187, 2003. [PubMed: 12706305]

5. Arriza JL, Weinberger C, Cerelli G, Glaser TM, Handelin BL, Housman DE, Evans RM. Cloning of human mineralocorticoid receptor complementary DNA: structural and functional kinship with the glucocorticoid receptor. Science 237: 268–275, 1987. [PubMed: 3037703]

6. Atanasov AG, Ignatova ID, Nashev LG, Dick B, Ferrari P, Frey FJ, Odermatt A. Impaired protein stability of 11beta-hydroxysteroid dehydrogenase type 2: a novel mechanism of apparent mineralocorticoid excess. J Am Soc Nephrol 18: 1262–1270, 2007. [PubMed: 17314322]

7. Azzi A, Rehse PH, Zhu DW, Campbell RL, Labrie F, Lin SX. Crystal structure of human estrogenic 17beta-hydroxysteroid dehydrogenase complexed with 17beta-estradiol. Nat Struct Biol 3: 665–668, 1996. [PubMed: 8756321]

8. Berman HM, Westbrook J, Feng Z, Gilliland G, Bhat TN, Weissig H, Shindyalov IN, Bourne PE. The Protein Data Bank. Nucleic Acids Res 28: 235–242, 2000. [PMCID: PMC102472] [PubMed: 10592235]

9. Brand E, Kato N, Chatelain N, Krozowski ZS, Jeunemaitre X, Corvol P, Plouin PF, Cambien F, Pascoe L, Soubrier F. Structural analysis and evaluation of the 11beta-hydroxysteroid dehydrogenase type 2 (11beta-HSD2) gene in human essential hypertension. J Hypertens 16: 1627–1633, 1998. [PubMed: 9856363]

10. Bray JE, Marsden BD, Oppermann U. The human short-chain dehydrogenase/reductase (SDR) superfamily: a bioinformatics summary. Chem Biol Interact 178: 99–109, 2009. [PubMed: 19061874]

11. Brown RW, Chapman KE, Murad P, Edwards CR, Seckl JR. Purification of 11beta-hydroxysteroid dehydrogenase type 2 from human placenta utilizing a novel affinity labelling technique. Biochem J 313: 997–1005, 1996. [PMCID: PMC1217009] [PubMed: 8611186]

12. Carvajal CA, Gonzalez AA, Romero DG, Gonzalez A, Mosso LM, Lagos ET, Hevia MDP, Rosati MP, Perez-Acle TO, Gomez-Sanchez CE, Montero JA, Fardella CE. Two homozygous mutations in the 11beta-hydroxysteroid dehydrogenase type 2 gene in a case of apparent mineralocorticoid excess. J Clin Endocrinol Metab 88: 2501–2507, 2003. [PubMed: 12788846]

13. Carvajal CA, Romero DG, Mosso LM, Gonzalez AA, Campino C, Montero J, Fardella CE. Biochemical and genetic characterization of 11beta-hydroxysteroid dehydrogenase type 2 in low-renin essential hypertensives. J Hypertens 23: 71–77, 2005. [PubMed: 15643127]

14. Coeli FB, Ferraz LFC, Lemos-Marini SHVD, Rigatto SZP, Belangero VMS, de-Mello MP. Apparent mineralocorticoid excess syndrome in a Brazilian boy caused by the homozygous missense mutation p.R186C in the HSD11B2 gene. Arq Bras Endocrinol Metabol 52: 1277–1281, 2008. [PubMed: 19169481]

15. Cole C, Barber JD, Barton GJ. The Jpred 3 secondary structure prediction server. Nucleic Acids Res 36: W197–W201, 2008. [PMCID: PMC2447793] [PubMed: 18463136]

16. Cristobal S, Zemla A, Fischer D, Rychlewski L, Elofsson A. A study of quality measures for protein threading models. BMC Bioinformatics 2: 5, 2001. [PMCID: PMC55330] [PubMed: 11545673]

17. Dave-Sharma S, Wilson RC, Harbison MD, Newfield R, Azar MR, Krozowski ZS, Funder JW, Shackleton CH, Bradlow HL, Wei JQ, Hertecant J, Moran A, Neiberger RE, Balfe JW, Fattah A, Daneman D, Akkurt HI, Santis CD, New MI. Examination of genotype and phenotype relationships in 14 patients with apparent mineralocorticoid excess. J Clin Endocrinol Metab 83: 2244–2254, 1998. [PubMed: 9661590]

18. DeLano WL. The PyMOL Molecular Graphics System [online]. 2002. http://www.pymol.org.

19. Ehrensberger AH, Elling RA, Wilson DK. Structure-guided engineering of xylitol dehydrogenase cosubstrate specificity. Structure 14: 567–575, 2006. [PubMed: 16531240]

20. Ferrari P, Obeyesekere VR, Li K, Andrews RK, Krozowski ZS. The 11beta-hydroxysteroid dehydrogenase type II enzyme: biochemical consequences of the congenital R337C mutation. Steroids 61: 197–200, 1996. [PubMed: 8733000]

21. Ferrari P, Obeyesekere VR, Li K, Wilson RC, New MI, Funder JW, Krozowski ZS. Point mutations abolish 11beta-hydroxysteroid dehydrogenase type II activity in three families with the congenital syndrome of apparent mineralocorticoid excess. Mol Cell Endocrinol 119: 21–24, 1996. [PubMed: 8793850]

22. Fiser A, Sali A. ModLoop: automated modeling of loops in protein structures. Bioinformatics 19: 2500–2501, 2003. [PubMed: 14668246]

23. Frishman D, Argos P. Knowledge-based protein secondary structure assignment. Proteins 23: 566–579, 1995. [PubMed: 8749853]

24. Funder JW, Pearce PT, Smith R, Smith AI. Mineralocorticoid action: target tissue specificity is enzyme, not receptor, mediated. Science 242: 583–585, 1988. [PubMed: 2845584]

25. Gangloff A, Shi R, Nahoum V, Lin S. Pseudo-symmetry of C19 steroids, alternative binding

orientations, and multispecificity in human estrogenic 17beta-hydroxysteroid dehydrogenase. FASEB J 17: 274–276, 2003. [PubMed: 12490543]

26. Ghosh D, Sawicki M, Pletnev V, Erman M, Ohno S, Nakajin S, Duax WL. Porcine carbonyl reductase. Structural basis for a functional monomer in short chain dehydrogenases/reductases. J Biol Chem 276: 18457–18463, 2001. [PubMed: 11279087]

27. Ghosh D, Vihkoz P. Molecular mechanisms of estrogen recognition and 17-keto reduction by human 17beta-hydroxysteroid dehydrogenase 1. Chem Biol Interact 130–132: 637–650, 2001.

28. Gomez-Sanchez EP, Ganjam V, Chen YJ, Liu Y, Clark SA, Gomez-Sanchez CE. The 11beta hydroxysteroid dehydrogenase 2 exists as an inactive dimer. Steroids 66: 845–848, 2001. [PubMed: 11576624]

29. Henrick K, Thornton JM. PQS: a protein quaternary structure file server. Trends Biochem Sci 23: 358–361, 1998. [PubMed: 9787643]

30. Hubbard TJP, Aken BL, Ayling S, Ballester B, Beal K, Bragin E, Brent S, Chen Y, Clapham P, Clarke L, Coates G, Fairley S, Fitzgerald S, Fernandez-Banet J, Gordon L, Graf S, Haider S, Hammond M, Holland R, Howe K, Jenkinson A, Johnson N, Kahari A, Keefe D, Keenan S, Kinsella R, Kokocinski F, Kulesha E, Lawson D, Longden I, Megy K, Meidl P, Overduin B, Parker A, Pritchard B, Rios D, Schuster M, Slater G, Smedley D, Spooner W, Spudich G, Trevanion S, Vilella A, Vogel J, White S, Wilder S, Zadissa A, Birney E, Cunningham F, Curwen V, Durbin R, Fernandez-Suarez XM, Herrero J, Kasprzyk A, Proctor G, Smith J, Searle S, Flicek P. Ensembl 2009. Nucleic Acids Res 37: D690–D697, 2009. [PMCID: PMC2686571] [PubMed: 19033362]

31. Kamide K, Kokubo Y, Hanada H, Nagura J, Yang J, Takiuchi S, Tanaka C, Banno M, Miwa Y, Yoshii M, Matayoshi T, Yasuda H, Horio T, Okayama A, Tomoike H, Kawano Y, Miyata T. Genetic variations of HSD11B2 in hypertensive patients and in the general population, six rare missense/frameshift mutations. Hypertens Res 29: 243–252, 2006. [PubMed: 16778331]

32. Kelley LA, Sternberg MJE. Protein structure prediction on the Web: a case study using the Phyre server. Nat Protoc 4: 363–371, 2009. [PubMed: 19247286]

33. Kitanaka S, Katsumata N, Tanae A, Hibi I, Takeyama K, Fuse H, Kato S, Tanaka T. A new compound heterozygous mutation in the 11beta-hydroxysteroid dehydrogenase type 2 gene in a case of apparent mineralocorticoid excess. J Clin Endocrinol Metab 82: 4054–4058, 1997. [PubMed: 9398712]

34. Kotelevtsev Y, Brown RW, Fleming S, Kenyon C, Edwards CR, Seckl JR, Mullins JJ. Hypertension in mice lacking 11beta-hydroxysteroid dehydrogenase type 2. J Clin Invest 103: 683–689, 1999. [PMCID: PMC408118] [PubMed: 10074485]

35. Kristan K, Deluca D, Adamski J, Stojan J, Rizner TL. Dimerization and enzymatic activity of fungal 17beta-hydroxysteroid dehydrogenase from the short-chain dehydrogenase/reductase superfamily. BMC Biochem 6: 28, 2005. [PMCID: PMC1326212] [PubMed: 16359545]

36. Lavery GG, Ronconi V, Draper N, Rabbitt EH, Lyons V, Chapman KE, Walker EA, McTernan CL, Giacchetti G, Mantero F, Seckl JR, Edwards CRW, Connell JMC, Hewison M, Stewart PM. Late-onset apparent mineralocorticoid excess caused by novel compound heterozygous mutations in the HSD11B2 gene. Hypertension 42: 123–129, 2003. [PubMed: 12860834]

37. Li A, Li KX, Marui S, Krozowski ZS, Batista MC, Whorwood CB, Arnhold IJ, Shackleton CH, Mendonca BB, Stewart PM. Apparent mineralocorticoid excess in a Brazilian kindred: hypertension in

the heterozygote state. J Hypertens 15: 1397–1402, 1997. [PubMed: 9431844]

38. Li A, Tedde R, Krozowski ZS, Pala A, Li KX, Shackleton CH, Mantero F, Palermo M, Stewart PM. Molecular basis for hypertension in the “type II variant” of apparent mineralocorticoid excess. Am J Hum Genet 63: 370–379, 1998. [PMCID: PMC1377297] [PubMed: 9683587]

39. Lin-Su K, Zhou P, Arora N, Betensky BP, New MI, Wilson RC. In vitro expression studies of a novel mutation delta299 in a patient affected with apparent mineralocorticoid excess. J Clin Endocrinol Metab 89: 2024–2027, 2004. [PubMed: 15126515]

40. Lovati E, Ferrari P, Dick B, Jostarndt K, Frey BM, Frey FJ, Schorr U, Sharma AM. Molecular basis of human salt sensitivity: the role of the 11beta-hydroxysteroid dehydrogenase type 2. J Clin Endocrinol Metab 84: 3745–3749, 1999. [PubMed: 10523024]

41. Lovell SC, Davis IW, Arendall WB, Bakker PIWD, Word JM, Prisant MG, Richardson JS, Richardson DC. Structure validation by Calpha geometry: phi, psi and Cbeta deviation. Proteins 50: 437–450, 2003. [PubMed: 12557186]

42. Lüthy R, Bowie JU, Eisenberg D. Assessment of protein models with three-dimensional profiles. Nature 356: 83–85, 1992. [PubMed: 1538787]

43. Mariniello B, Ronconi V, Sardu C, Pagliericcio A, Galletti F, Strazzullo P, Palermo M, Boscaro M, Stewart PM, Mantero F, Giacchetti G. Analysis of the 11beta-hydroxysteroid dehydrogenase type 2 gene (HSD11B2) in human essential hypertension. Am J Hypertens 18: 1091–1098, 2005. [PubMed: 16109323]

44. Monder C, White PC. 11beta-Hydroxysteroid dehydrogenase. Vitam Horm 47: 187–271, 1993. [PubMed: 8447114]

45. Mune T, Rogerson FM, Nikkilä H, Agarwal AK, White PC. Human hypertension caused by mutations in the kidney isozyme of 11beta-hydroxysteroid dehydrogenase. Nat Genet 10: 394–399, 1995. [PubMed: 7670488]

46. Mune T, White PC. Apparent mineralocorticoid excess: genotype is correlated with biochemical phenotype. Hypertension 27: 1193–1199, 1996. [PubMed: 8641723]

47. Nunez BS, Rogerson FM, Mune T, Igarashi Y, Nakagawa Y, Phillipov G, Moudgil A, Travis LB, Palermo M, Shackleton C, White PC. Mutants of 11beta-hydroxysteroid dehydrogenase (11-HSD2) with partial activity: improved correlations between genotype and biochemical phenotype in apparent mineralocorticoid excess. Hypertension 34: 638–642, 1999. [PubMed: 10523339]

48. Obeid J, White PC. Tyr-179 and Lys-183 are essential for enzymatic activity of 11beta-hydroxysteroid dehydrogenase. Biochem Biophys Res Commun 188: 222–227, 1992. [PubMed: 1417845]

49. Obeyesekere VR, Ferrari P, Andrews RK, Wilson RC, New MI, Funder JW, Krozowski ZS. The R337C mutation generates a high K_m 11beta-hydroxysteroid dehydrogenase type II enzyme in a family with apparent mineralocorticoid excess. J Clin Endocrinol Metab 80: 3381–3383, 1995. [PubMed: 7593456]

50. Obeyesekere VR, Li KX, Ferrari P, Krozowski Z. Truncation of the N- and C-terminal regions of the human 11beta-hydroxysteroid dehydrogenase type 2 enzyme and effects on solubility and bidirectional enzyme activity. Mol Cell Endocrinol 131: 173–182, 1997. [PubMed: 9296376]

51. Odermatt A, Arnold P, Stauffer A, Frey BM, Frey FJ. The N-terminal anchor sequences of 11beta-hydroxysteroid dehydrogenases determine their orientation in the endoplasmic reticulum membrane. J Biol Chem 274: 28762–28770, 1999. [PubMed: 10497248]

52. Odermatt A, Dick B, Arnold P, Zaehner T, Plueschke V, Deregibus MN, Repetto H, Frey BM, Frey FJ, Ferrari P. A mutation in the cofactor-binding domain of 11beta-hydroxysteroid dehydrogenase type 2 associated with mineralocorticoid hypertension. J Clin Endocrinol Metab 86: 1247–1252, 2001. [PubMed: 11238516]

53. Persson B, Kallberg Y, Bray JE, Bruford E, Dellaporta SL, Favia AD, Duarte RG, Jörnvall H, Kavanagh KL, Kedishvili N, Kisiela M, Maser E, Mindnich R, Orchard S, Penning TM, Thornton JM, Adamski J, Oppermann U. The SDR (short-chain dehydrogenase/reductase and related enzymes) nomenclature initiative. Chem Biol Interact 178: 94–98, 2009. [PMCID: PMC2896744] [PubMed: 19027726]

54. Poch E, González D, Giner V, Bragulat E, Coca A, de La Sierra A. Molecular basis of salt sensitivity in human hypertension. Evaluation of renin-angiotensin-aldosterone system gene polymorphisms. Hypertension 38: 1204–1209, 2001. [PubMed: 11711524]

55. Sali A, Blundell TL. Comparative protein modelling by satisfaction of spatial restraints. J Mol Biol 234: 779–815, 1993. [PubMed: 8254673]

56. Shen M, Sali A. Statistical potential for assessment and prediction of protein structures. Protein Sci 15: 2507–2524, 2006. [PMCID: PMC2242414] [PubMed: 17075131]

57. Smolenicka Z, Bach E, Schaer A, Liechti-Gallati S, Frey BM, Frey FJ, Ferrari P. A new polymorphic restriction site in the human 11beta-hydroxysteroid dehydrogenase type 2 gene. J Clin Endocrinol Metab 83: 1814–1817, 1998. [PubMed: 9589699]

58. Stewart PM, Corrie JE, Shackleton CH, Edwards CR. Syndrome of apparent mineralocorticoid excess. A defect in the cortisol-cortisone shuttle. J Clin Invest 82: 340–349, 1988. [PMCID: PMC303514] [PubMed: 3164727]

59. Stewart PM, Krozowski ZS, Gupta A, Milford DV, Howie AJ, Sheppard MC, Whorwood CB. Hypertension in the syndrome of apparent mineralocorticoid excess due to mutation of the 11beta-hydroxysteroid dehydrogenase type 2 gene. Lancet 347: 88–91, 1996. [PubMed: 8538347]

60. Thompson JD, Gibson TJ, Plewniak F, Jeanmougin F, Higgins DG. The CLUSTAL X windows interface: flexible strategies for multiple sequence alignment aided by quality analysis tools. Nucleic Acids Res 25: 4876–4882, 1997. [PMCID: PMC147148] [PubMed: 9396791]

61. Ulick S, Tedde R, Mantero F. Pathogenesis of the type 2 variant of the syndrome of apparent mineralocorticoid excess. J Clin Endocrinol Metab 70: 200–206, 1990. [PubMed: 2403571]

62. Vriend G, Sander C. Quality control of protein models: directional atomic contact analysis. J Appl Crystallogr 26: 47–60, 1993.

63. Wallner B, Elofsson A. Can correct protein models be identified? Protein Sci 12: 1073–1086, 2003. [PMCID: PMC2323877] [PubMed: 12717029]

64. Waterhouse AM, Procter JB, Martin DMA, Clamp M, Barton GJ. Jalview Version 2—a multiple sequence alignment editor and analysis workbench. Bioinformatics 25: 1189–1191, 2009. [PMCID: PMC2672624] [PubMed: 19151095]

65. Watson B, Bergman SM, Myracle A, Callen DF, Acton RT, Warnock DG. Genetic association of 11beta-hydroxysteroid dehydrogenase type 2 (HSD11B2) flanking microsatellites with essential hypertension in blacks. Hypertension 28: 478–482, 1996. [PubMed: 8794836]

66. Wilson RC, Dave-Sharma S, Wei JQ, Obeyesekere VR, Li K, Ferrari P, Krozowski ZS, Shackleton CH, Bradlow L, Wiens T, New MI. A genetic defect resulting in mild low-renin hypertension. Proc Natl Acad Sci USA 95: 10200–10205, 1998. [PMCID: PMC21485] [PubMed: 9707624]

67. Wilson RC, Harbison MD, Krozowski ZS, Funder JW, Shackleton CH, Hanauske-Abel HM, Wei JQ, Hertecant J, Moran A, Neiberger RE. Several homozygous mutations in the gene for 11beta-hydroxysteroid dehydrogenase type 2 in patients with apparent mineralocorticoid excess. J Clin Endocrinol Metab 80: 3145–3150, 1995. [PubMed: 7593417]

68. Wilson RC, Krozowski ZS, Li K, Obeyesekere VR, Razzaghy-Azar M, Harbison MD, Wei JQ, Shackleton CH, Funder JW, New MI. A mutation in the HSD11B2 gene in a family with apparent mineralocorticoid excess. J Clin Endocrinol Metab 80: 2263–2266, 1995. [PubMed: 7608290]

69. Yue P, Li Z, Moult J. Loss of protein structure stability as a major causative factor in monogenic disease. J Mol Biol 353: 459–473, 2005. [PubMed: 16169011]

Figures and Tables

Fig. 1.

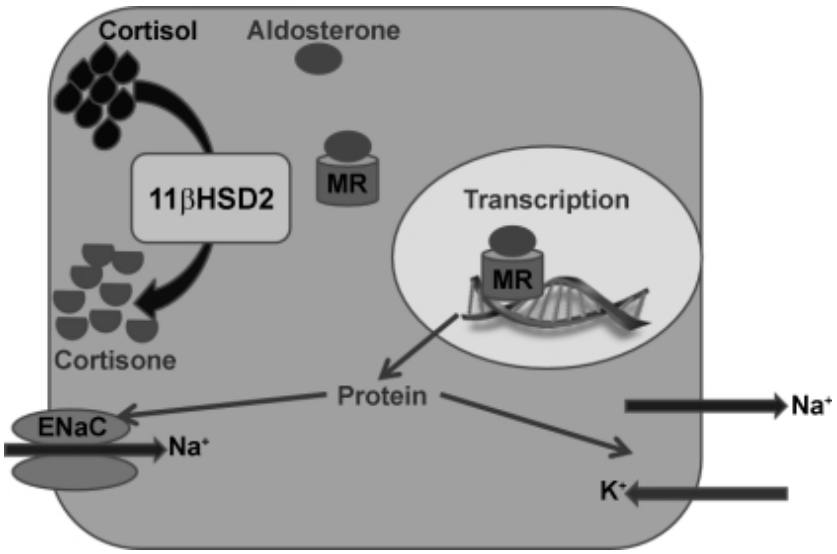

Outline of 11β-hydroxysteroid dehydrogenase type 2 (11βHSD2) mechanism. 11βHSD2 prevents activation of the mineralocorticoid receptor (MR) by cortisol, allowing aldosterone to bind with consequent downstream effects on transcription. ENaC, epithelial sodium channel. Figure credit: Louise Evans.

Fig. 2.

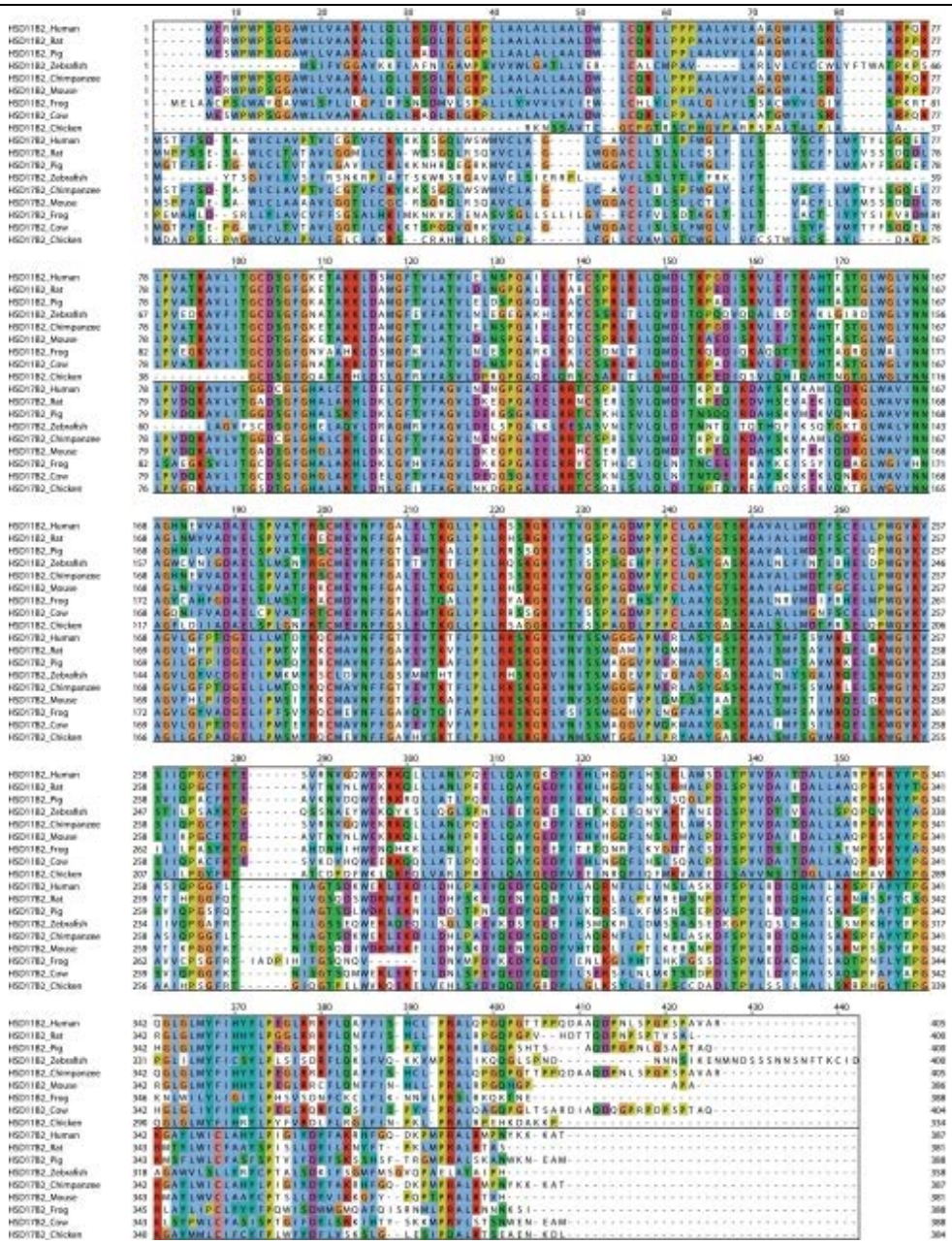

Multiple protein sequence alignment of 11βHSD2 enzymes and their immediate neighbors, the 17βHSD2s, adapted from the alignment for the Ensembl protein family ENSFM00500000270244. Figure prepared with Jalview (64) with ClustalX (60) coloring option.

Fig. 3.

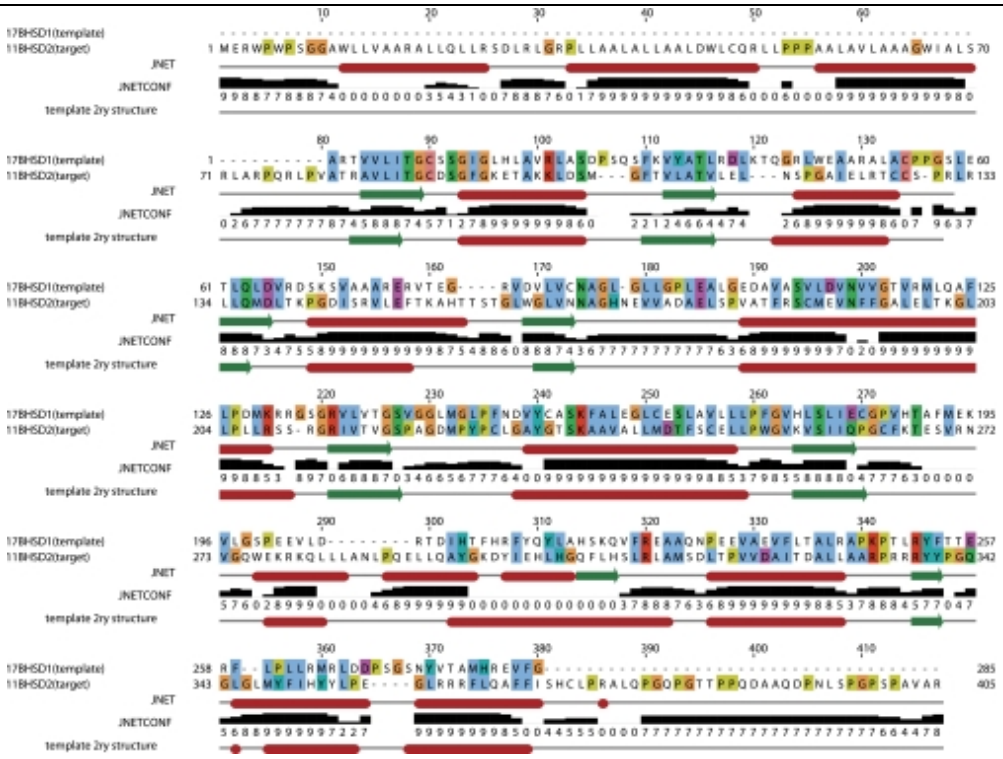

Pairwise sequence alignment of human 11βHSD2 with the template used for modeling, 17βHSD1 [PDB ID: 1JTV (25), chain A], showing only those template residues solved in the structure. Secondary structure is shown below the alignment, derived from the sequence via the secondary structure prediction server JPred (15) and from the template structure via Stride (23). JPred confidence scores for assignment of residues to secondary structure element are shown for the target sequence. Red, α-helices; green, β-strands. Figure created with Jalview (64), with ClustalX coloring. Numbers above sequences refer to alignment position, not sequence position.

Fig. 4.

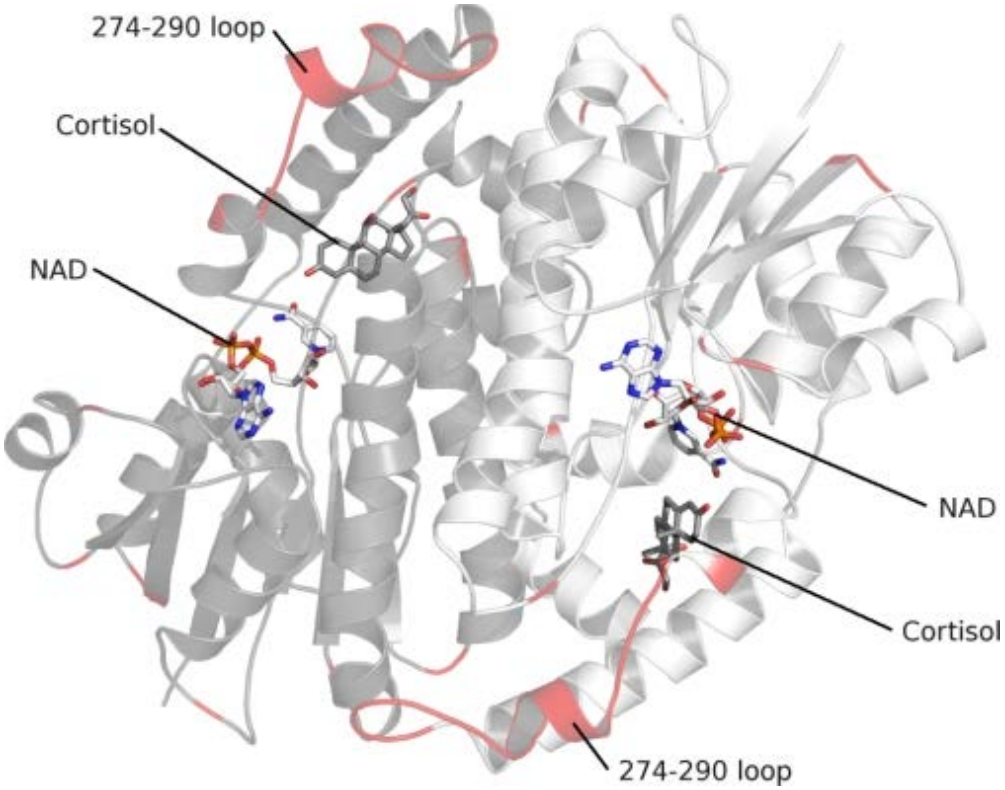

Dimeric 3-dimensional model of human 11βHSD2 based on human 17βHSD1. One monomer is shown in dark gray and the other in white, and both are depicted in cartoon representation. NAD is shown in stick form with carbons in white, while cortisol is shown in gray stick form. Other atoms are in standard color scheme (red, oxygen; blue, nitrogen; orange, phosphorus). Red cartoon regions highlight portions of the model with 1 or more identified problems in modeling.

Table 1.

Summary of mutations and associated phenotypic consequences

Mutation(s)	Location	Alignment Position	Reference	Heterozygous/Homozygous	Phenotype	Pr
Disease-associated mutations						
ΔTTGGAG	Exon 2	127 + 128	52	hom	AME	ΔL114+E115
CTG→CGG+	Exon 3 + Exon 4	192 + 259→	47	hom	AME	L179R+ fran
TCT→TTT	Exon 3	193	47	hom	AME	S180F
CGT→TCG	Exon 3	199	13, 67	hom	AME	R186C
CGC→TGC	Exon 3	229	45	hom	AME	R208C
CGC→CAC/CGCTAT→CAT	Exon 3/exon 5	221/356 + 357	33	het/het	AME	R208H/R33
CGC→CAC+ C→T	Exon 3 + intron 3	221	47	hom	AME	R208H+ Δe
CGC→TGC	Exon 3	226	45	hom	AME	R213C
GAC→AAC+ C→T	Exon 4 + intron 3	236	12	hom	AME	D223+ Δexo
A→+A→T/C→T	Exon 4/3′ UTR	246	36	het/het	AME	Y226N/–
A→G+A→T	Exon 4	239	36	het	LOH	Y226N
CCG→CTG	Exon 4	240	66	hom	AME (mild)	P227L
Δ9bp/Δ11bp	Exon 4/exon 5	245–247	45	het/het	AME	Y232S, Δ(G233+T23
TAT→TGT/CTG→CCG	Exon 4/exon 5	245/397	36	het/het	AME	Y232C/L376
GCG→GTG/GCG→GTG	Exon 4/exon 5	250/347	47	het/het	AME	A237V/A328

CTC→CGC/GAC→AAC	Exon 4/exon 4	263/257	17	het/het	AME	L250R/D24
CTCCTT→CCCTCT	Exon 4	263 + 264	45, 67	hom	AME	L250P+L251
C→T	Intron 3		45	hom	AME	ΔExon 4
CGC→TGC	Exon 5	298	38	hom het	AME (mild)†, LOH*	R279C
AAC→AA	Exon 5		17	hom	AME	N286 −1 fra
ΔTAC	Exon 5	318	39	hom	AME	ΔY299
GCG→GTG	Exon 5	347	37	hom/het	AME LOH	A328V
CGC→TGC	Exon 5	398	68	hom	AME	R337C
CGCTAT→CAT	Exon 5	356 + 357	45, 67	hom	AME	R337H+ΔY3
ΔCA/TAT→CTG	Exon 1/exon 5	32/357	6	het/het	AME	Truncation a
GAA→GTG	Exon 5	375 →	67	hom	AME	E356 frames
CGG→TGG/G→A	Exon 5/intron 3	378/–	36	het/het	AME (mild)	R359W/spli
CGG→TGG	Exon 5	378	36	het	LOH	R359W
CGA→TGA	Exon 5	395 →	59	hom	AME	R374Term
C→T	3′ UTR		36	het	LOH	
				Engineered mutations		
		245	48			Y232F
		245	48			Y232S
		249	48			K236R
		104	48			D91N
	Exon 2	128	52			E115G
	Exon 2	128	52			E115K
	Exon 5	396	6			R335K
		354	6			R335Q
		354	6			R335A
		355	6			R336K
		355	6			R336Q

355	6	R336A
356	6	R337K
356	6	R337Q
356	6	R337A
399	6	R338F
399	6	R338A
400	6	R339F
400	6	R339A
400	6	R339H

References are cited for the discovery of each mutation and separately for the in vitro activity, where appropriate. Activities are shown as a qualitative guide to indicate where partial enzymatic activity may be retained by mutant proteins; however, quantitative assessments involving these values would be unwise because of differences in experimental procedures, metrics of activity, etc.

AME, apparent mineralocorticoid excess; LOH, late-onset hypertension; UTR, untranslated region. Multiple mutations are indicated by "/"' for compound heterozygotes, "+" for compound homozygotes. Alignment positions relative to Fig. 2 are included for ease of cross-referencing.

*Patient lacked mineralocorticoid excess.
†Patients had syndrome sometimes referred to as "type II" AME, characterized by AME symptoms but mild biochemical phenotype.
‡Activity measured from placental homogenate relative to control.

Fig. 5.

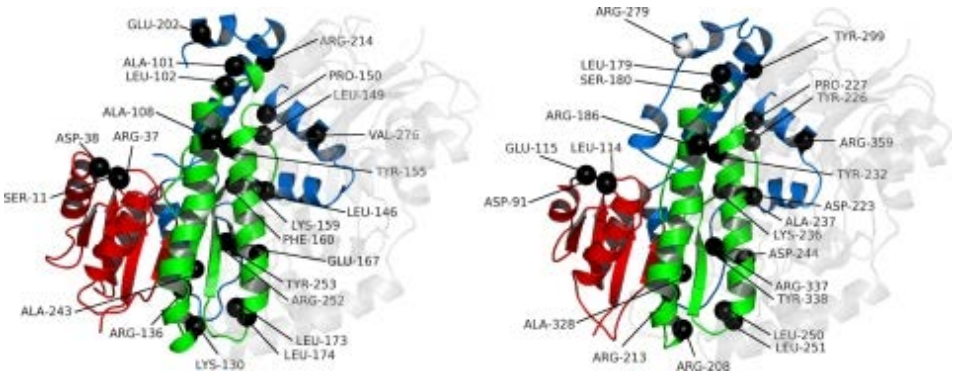

The model 11βHSD2 (*right*) compared with the template 17βHSD1 (*left*) with location of mutations mapped. One chain is split by color to separate major groups of secondary structure elements. The main cofactor-binding domain is shown in red at the NH_2 terminus, 2 long helices that support much of the active site are shown in green, and the COOH-terminal region is shown in blue. Note: a short segment (amino acids 191–197) was not solved in the template [PDB ID: 1JTV (25)], seen at *top left*. Spheres indicate the α-carbon positions of pathogenic mutations or their equivalents in the template—only mapped on 1 chain for clarity. White spheres indicate potential problems at these positions during modeling (see text).

Fig. 6.

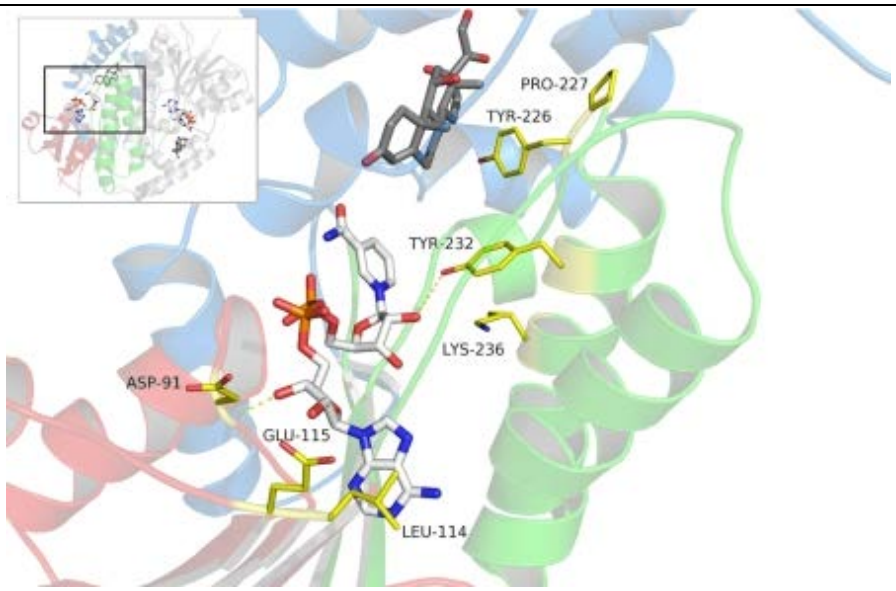

Residues important for function or associated with apparent mineralocorticoid excess (AME) on mutation around the substrate and cofactor binding regions. The side chains of residues involved in pathogenic mutation are shown in yellow stick form. Dashed yellow lines indicate predicted hydrogen bonds. The location of this region with respect to the overall model dimer is shown in the *inset*. Protein chains are colored as in Fig. 5 and ligands as in Fig. 4.

Fig. 7.

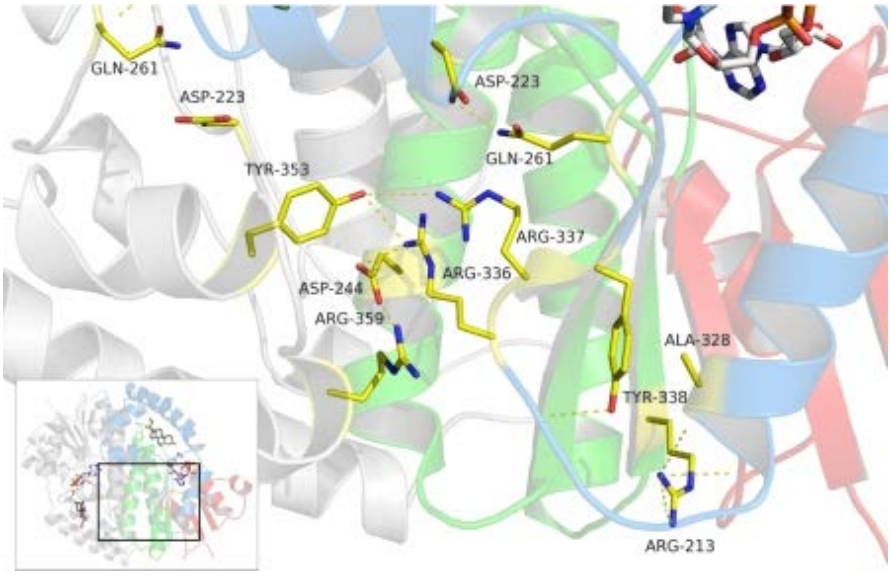

Residues involved in AME-associated mutations that may affect protein stability are shown labeled. The dimer is rotated 180° relative to Fig. 5. Color scheme and formatting as in previous figures.

Fig. 8.

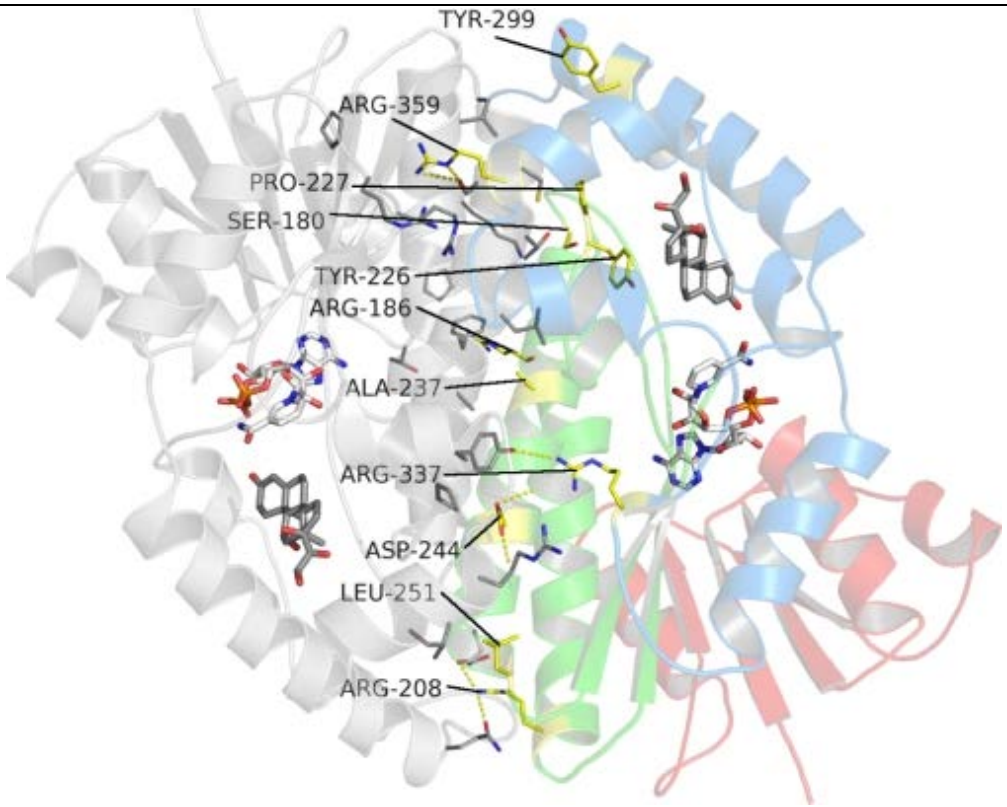

Residues involved in AME-associated mutations that occur at the dimer interface are indicated. The dimer is rotated 180° relative to Fig. 5. Color scheme as in previous figures.

Fig. 9.

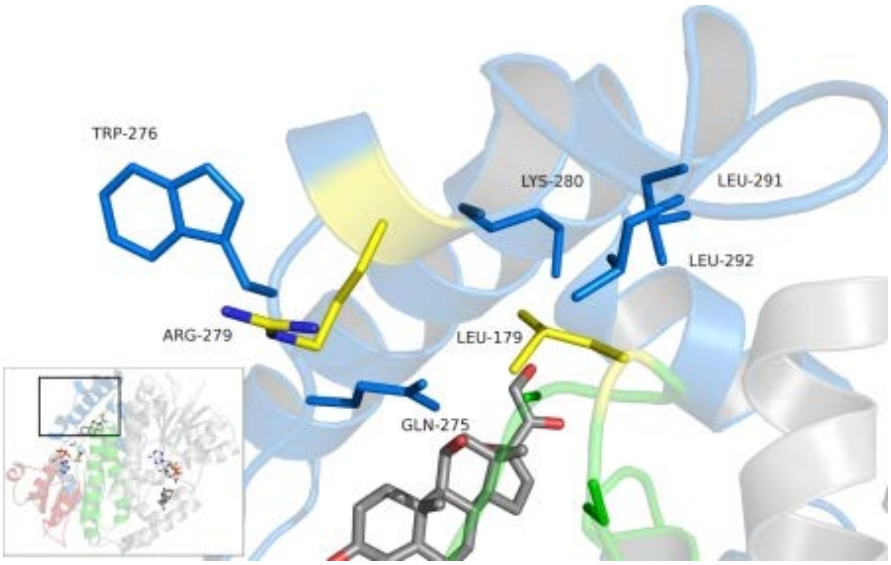

Residues involved in AME-associated mutations that were not classified are shown. As indicated in the *inset*, the dimer is shown in the same orientation as Fig. 5.